Controllability Methods for the Calculation of Time-Periodic Solutions. Application to Scattering.

Marie-Odile Bristeau, Roland Glowinski, Jacques Périaux

▶ **To cite this version:**

Marie-Odile Bristeau, Roland Glowinski, Jacques Périaux. Controllability Methods for the Calculation of Time-Periodic Solutions. Application to Scattering.. [Research Report] RR-3386, INRIA. 1998. ⟨inria-00073303⟩

HAL Id: inria-00073303

https://inria.hal.science/inria-00073303v1

Submitted on 24 May 2006

HAL is a multi-disciplinary open access archive for the deposit and dissemination of scientific research documents, whether they are published or not. The documents may come from teaching and research institutions in France or abroad, or from public or private research centers.

L'archive ouverte pluridisciplinaire **HAL**, est destinée au dépôt et à la diffusion de documents scientifiques de niveau recherche, publiés ou non, émanant des établissements d'enseignement et de recherche français ou étrangers, des laboratoires publics ou privés.

HAL Authorization

INRIA

INSTITUT NATIONAL DE RECHERCHE EN INFORMATIQUE ET EN AUTOMATIQUE

Controllability Methods for the Calculation of Time-Periodic Solutions. Application to Scattering.

Marie-Odile Bristeau , Roland Glowinski , Jacques Périaux

No 3386

Mars 1998

THÈME 4

ISSN 0249-6399

INRIA
ROCQUENCOURT

Controllability Methods for the Calculation of Time-Periodic Solutions. Application to Scattering.

Marie-Odile Bristeau , * Roland Glowinski , † Jacques Périaux ‡

Thème 4 — Simulation et optimisation
de systèmes complexes
Projet M3N

Rapport de recherche n ° 3386 — Mars 1998 — 43 pages

Abstract: We discuss in this article the application of controllability techniques to the calculation of the time-periodic solutions of evolution equations. The basic principles of the computational methods are presented in a fairly general context where we discuss the time discretization aspect. We apply then this general methodology to the solution of scattering problems for harmonic planar waves by two and three dimensional purely reflecting non-convex obstacles. Numerical results obtained by the above method and comparisons with the results obtained by more classical methods show the superiority of the former ones. In annexe A, we give some details on the Radar Cross Section computation.

Key-words: Time-periodic solutions, Controllability, Least-Squares /Shooting method, Conjugate Gradient, Scattering.

(Résumé : tsvp)

* M3N, Email : Marie-Odile.Bristeau@inria.fr
† Dept. of Mathematics, University of Houston, Houston, Texas 77204-3476, U.S.A.
‡ Dassault Aviation, 78, quai M. Dassault, 92214 Saint-Cloud, France

Unité de recherche INRIA Rocquencourt
Domaine de Voluceau, Rocquencourt, BP 105, 78153 LE CHESNAY Cedex (France)
Téléphone : 01 39 63 55 11 - International : +33 1 39 63 55 11
Télécopie : (33) 01 39 63 53 30 - International : +33 1 39 63 53 30

Méthodes de Contrôlabilité pour le calcul de solutions périodiques en temps. Application à la diffraction.

Résumé : Dans cet article, on étudie l'application de techniques de contrôlabilité au calcul de solutions périodiques de problèmes d'évolution. Les principes de base de ces méthodes de calcul sont présentés dans un contexte assez général, l'aspect discrétisation en temps est aussi abordé. On applique ensuite cette méthodologie à la résolution de problèmes de diffraction d'ondes planes harmoniques par des obstacles non-convexes bi- et tri-dimensionnels parfaitement réfléchissants. La comparaison des résultats obtenus par cette méthode avec ceux obtenus par des méthodes plus classiques montre l'efficacité de la première. L'annexe A contient quelques precisions sur le calcul de la S.E.R..

Mots-clé : Solutions périodiques, Contrôlabilité, Moindres-Carrés/Méthode de tir, Gradient Conjugué, Diffraction.

Introduction and Synopsis

A decade ago (at a conference organized in Florida by I. Lascieka and R. Triggiani ; see ref. [1]), we discussed in [2] some application of control principles and methods to the calculation of *time-periodic solutions* of evolution equations (possibly nonlinear with the period known or unknown). The method used at the time was and still is of the *least-squares/shooting* type and was taking advantage of the control *formalism* and *methodology*.

Several applications have been considered since the publication of [2], including the simulation of the *scattering* of *harmonic planar waves* by reflecting or dielectrically coated convex or non-convex bodies (see refs. [3]-[6]). Other applications have been considered by G. Auchmuty et al. [7] and we are presently investigating the time-periodic solutions of systems of highly nonlinear parabolic equations of the advection-reaction-diffusion type from chemical engineering. In the present article after a presentation of the method principles in a general context, we will discuss the application to the solution of complicated scattering problems in two and three space dimensions which are not easily solved by more classical methods. Actually we shall take advantage of the present article to show comparisons with results from an alternative method recently introduced by Bardos and Rauch in [8].

1 Time-periodic solutions of evolution linear equations

Let us consider the following problem

$$\left\{ \begin{array}{l} \dfrac{dy}{dt} + Ay = f, \\ y(0) = y(T), \end{array} \right. \tag{1.1}$$

with $A \in \mathcal{L}(V, V')$ and f a T-periodic forcing function. We suppose that V is a real Hilbert space and that V' is its dual space. We do not discuss here the existence and uniqueness of solutions to (1.1).

2 An exact controllability formulation

We suppose that the *Cauchy problem*

$$\left\{ \begin{array}{l} \dfrac{dy}{dt} + Ay = f, \\ y(0) = y_0, \end{array} \right. \tag{2.1}$$

has a unique solution on $(0,T), \forall y_0 \in H$ (with $V \subset H \subset V', \bar{V}^H = H$) and also that $y \in C^0([0,T];H)$ (here H is also an Hilbert space).

Problem (1.1) is clearly equivalent to finding e such that

$$\left\{ \begin{array}{l} e \in H, \\ \dfrac{dy}{dt} + Ay = f, \\ y(0) = e, y(T) = e. \end{array} \right. \tag{2.2}$$

3 A least-squares/shooting method

In order to solve problem (2.2) we suggest the following *least-squares/shooting* approach where instead of solving (2.2) "directly" we substitute to it the following *minimization* problem

$$e \in H, \quad J(e) \leq J(v), \forall v \in H, \tag{3.1}$$

with

$$J(v) = \frac{1}{2}|y(T) - v|^2, \tag{3.2}$$

where y is the solution of the initial value problem

$$\left\{ \begin{array}{l} \dfrac{dy}{dt} + Ay = f, \\ y(0) = v; \end{array} \right. \tag{3.3}$$

in (3.2) $|.|$ denotes the H-norm (we denote by $(.,.)$ the corresponding scalar product).

There is equivalence between (1.1) and (3.1) if and only if $J(e) = 0$.

4 Optimality conditions for problem (3.1)

If problem (3.1) has a solution e, we clearly have

$$J'(e) = 0. \tag{4.1}$$

In order to compute J' we shall use the following classical perturbation analysis :

Let δv be a perturbation of $v \in H$; we have then

$$\delta J(v) = (J'(v), \delta v). \tag{4.2}$$

We also have

$$\left\{ \begin{array}{ll} \delta J(v) & = (y(T) - v, \delta y(T) - \delta v) \\ & = (y(T) - v, \delta y(T)) + (v - y(T), \delta v). \end{array} \right. \tag{4.3}$$

The perturbation δy of y satisfies

$$\left\{ \begin{array}{l} \dfrac{d\delta y}{dt} + A\delta y = 0, \\ \delta y(0) = \delta v. \end{array} \right. \tag{4.4}$$

Consider now p so that $p \in L^2(0,T;V), \dfrac{dp}{dt} \in L^2(0,T;V')$ (which implies that $p \in C^o([0,T];H)$). Denoting by $< .,. >$ the duality pairing between V' and V, which coincides with $(.,.)$ if the first argument is smooth enough, we obtain from (4.4) that

$$\int_0^T < \frac{d}{dt}\delta y, p > dt + \int_0^T < A\delta y, p > dt = 0. \tag{4.5}$$

Integrating by parts, we obtain from (4.5) that

$$\left\{ \begin{array}{ll} -\displaystyle\int_0^T < \frac{dp}{dt}, \delta y > dt + \int_0^T < A^*p, \delta y > dt & = (p(0), \delta y(0)) - (p(T), \delta y(T)) \\ & = (p(0), \delta v) - (p(T), \delta y(T)). \end{array} \right. \tag{4.6}$$

Suppose that p satisfies the following *(adjoint)* equation

$$\left\{ \begin{array}{l} -\dfrac{dp}{dt} + A^*p = 0, \\ p(T) = y(T) - v; \end{array} \right. \tag{4.7}$$

it follows then from (4.2), (4.3), (4.6) that

$$J'(v) = v - y(T) + p(0). \tag{4.8}$$

From the *convexity* of the cost function J, condition (4.1) is a *necessary and sufficient optimality condition* which implies that e is solution of problem (3.1) if and only if the triple $\{e, y, p\}$ satisfies

$$e = y(T) - p(0), \tag{4.10}$$

$$\left\{ \begin{array}{l} \dfrac{dy}{dt} + Ay = f, \\ y(0) = e, \end{array} \right. \tag{4.11}$$

$$\left\{ \begin{array}{l} -\dfrac{dp}{dt} + A^* p = 0, \\ p(T) = y(T) - e. \end{array} \right. \tag{4.12}$$

There are several methods to solve system (4.10)-(4.12) ; one of the most efficient is the conjugate gradient algorithm to be described in the following paragraph.

5 Conjugate gradient solution of problem (3.1)

Operator $J' : H \to H$ being *affine*, solving equation (4.1) is equivalent to solving a linear problem in H. We can easily show that the *linear part* of J', namely operator

$$v \to J'(v) - J'(0)$$

is *symmetric* and *positive semi-definite* over H. From these properties conjugate gradient algorithms are natural candidates for solving problem (3.1), (4.1). Such an algorithm is described as follows

$$e^o \text{ is given in } H; \tag{5.1}$$

solve

$$\left\{ \begin{array}{l} \dfrac{dy^o}{dt} + Ay^o = f, \\ y^o(0) = e^o, \end{array} \right. \tag{5.2}$$

$$\left\{ \begin{array}{l} -\dfrac{dp^o}{dt} + A^* p^o = 0, \\ p^o(T) = y^o(T) - e^o, \end{array} \right. \tag{5.3}$$

$$\left\{ \begin{array}{l} g^o \in H, \\ (g^o, v) = (e^o - y^o(T) + p^o(0), v), \forall v \in H, \end{array} \right. \tag{5.4}$$

and set

$$w^o = g^o. \qquad \blacksquare \tag{5.5}$$

For $k \geq 0, e^k, g^k, w^k$ being known, compute $e^{k+1}, g^{k+1}, w^{k+1}$ as follows :

Solve

$$\left\{ \begin{array}{l} \dfrac{d\bar{y}^k}{dt} + A\bar{y}^k = 0, \\ \\ \bar{y}^k(0) = w^k, \end{array} \right. \tag{5.6}$$

$$\left\{ \begin{array}{l} -\dfrac{d\bar{p}^k}{dt} + A^*\bar{p}^k = 0, \\ \\ \bar{p}^k(T) = \bar{y}^k(T) - w^k, \end{array} \right. \tag{5.7}$$

$$\left\{ \begin{array}{l} \bar{g}^k \in H, \\ (\bar{g}^k, v) = (w^k - \bar{y}^k(T) + \bar{p}^k(0), v), \forall v \in H; \end{array} \right. \tag{5.8}$$

compute

$$\rho_k = \frac{|g^k|^2}{(\bar{g}^k, w^k)}, \tag{5.9}$$

and then

$$e^{k+1} = e^k - \rho_k w^k, \tag{5.10}$$

$$g^{k+1} = g^k - \rho_k \bar{g}^k. \tag{5.11}$$

If $|g^{k+1}|/|g^o| \leq \varepsilon$ take $e = e^{k+1}$; else, compute

$$\gamma_k = |g^{k+1}|^2/|g^k|^2, \tag{5.12}$$

and then

$$w^{k+1} = g^{k+1} + \gamma_k w^k. \tag{5.13}$$ ■

Do $k+1 \to k$ and return to (5.6).

Remark 5.1 : The choice of ε is *machine dependent* ; typical values range from

10^{-6} to 10^{-8}.

Remark 5.2 : We can use a stopping criterium based on $|y^{k+1}(T) - e^{k+1}|$, a quantity that we expect to converge to zero.

Remark 5.3 : The above algorithm can be viewed as an *impulse control* method for the equation

$$\frac{dy}{dt} + Ay = f$$

where we use the *periodicity defect* $y^k(T) - e^k$ to force the T-periodicity of the solution as $t \to +\infty$.

6 Time discretization

Let $\Delta t = T/N$ (N : a positive integer) be a *time discretization step.* We *formally* approximate problem (3.1) by

$$\begin{cases} e^{\Delta t} \in H, \\ J_{\Delta t}(e^{\Delta t}) \leq J_{\Delta t}(v), \forall v \in H, \end{cases} \tag{6.1}$$

where

$$J_{\Delta t}(v) = \frac{1}{2}|y^N - v|^2, \tag{6.2}$$

with y^n being obtained from v, for $n = 0, 1, \ldots, N$, by the following *forward Euler* time discretization scheme of (3.3)

$$\begin{cases} y^o = v; \\ for\ n = 1, \ldots, N, \\ \dfrac{y^n - y^{n-1}}{\Delta t} + Ay^{n-1} = f^{n-1}. \end{cases} \tag{6.3}$$

Remark 6.1 : If H is *infinite dimensional* and A *unbounded* over H, which is a typical situation if A is a *partial differential equation operator,* the above scheme is *unconditionally unstable.* However scheme (6.3) makes sense for Δt *sufficiently small* once V, H, A, f, y and v have been properly approximated by related *finite dimensional* mathematical objects.

Remark 6.2 : We have chosen the above scheme because its simplicity makes it very attractive in many complicated engineering applications. ■

Assuming that the discrete least-squares problem (6.1) has a solution $e^{\Delta t}$, this solution is characterized by

$$J'_{\Delta t}(e^{\Delta t}) = 0. \tag{6.4}$$

In order to compute $J'_{\Delta t}$ we proceed essentially as in the continuous case :
We observe that

$$\delta J_{\Delta t}(v) = (J'_{\Delta t}(v), \delta v), \tag{6.5}$$

and also that

$$\delta J_{\Delta t}(v) = (v - y^N, \delta v) + (y^N - v, \delta y^N), \tag{6.6}$$

with $\{\delta y^n\}_{n=0}^N$ satisfying (from (6.3))

$$\begin{cases} \delta y^o = \delta v; \\ for\ n = 1, \ldots, N, \\ \dfrac{\delta y^n - \delta y^{n-1}}{\Delta t} + A\delta y^{n-1} = 0. \end{cases} \tag{6.7}$$

Consider now $\{p^n\}_{n=1}^N \in V^N$; it follows from (6.7) that

$$\Delta t \sum_{n=1}^{N} (\frac{\delta y^n - \delta y^{n-1}}{\Delta t}, p^n) + \Delta t \sum_{n=1}^{N} < A^* p^n, \delta y^{n-1} >= 0. \tag{6.8}$$

Performing now a *discrete integration by parts*, we obtain from (6.7), (6.8)

$$(p^N, \delta y^N) + \Delta t \sum_{n=1}^{N-1} < \frac{p^n - p^{n+1}}{\Delta t} + A^* p^{n+1}, \delta y^n >= ((I - \Delta t A^*)p^1, \delta v). \tag{6.9}$$

Suppose that $\{p^n\}_{n=0}^N$ satisfies

$$\begin{cases} p^N = y^N - v; \\ for\ n = N-1, \ldots, 0, \\ \dfrac{p^n - p^{n+1}}{\Delta t} + A^* p^{n+1} = 0; \end{cases} \tag{6.10}$$

it follows from (6.5), (6.6), (6.9) that

$$J'_{\Delta t}(v) = v - y^N + p^o, \tag{6.11}$$

which is clearly the discrete analogue of (4.8) that we could expect.

Combining (6.4) to (6.11) we obtain the following *discrete optimality conditions* satisfied by the triple $e^{\Delta t}, \{y^n\}_{n=0}^N, \{p^n\}_{n=0}^N$

$$e^{\Delta t} = y^N - p^o, \tag{6.12}$$

$$\begin{cases} y^o = e^{\Delta t}; \\ for\ n = 1, \ldots, N \\ \dfrac{y^n - y^{n-1}}{\Delta t} + Ay^{n-1} = f^{n-1}, \end{cases} \tag{6.13}$$

$$\begin{cases} p^N = y^N - e^{\Delta t}; \\ for\ n = N-1, \ldots, 0, \\ \dfrac{p^n - p^{n+1}}{\Delta t} + A^* p^{n+1} = 0. \end{cases} \tag{6.14}$$

Following Section 5, we can derive from relations (6.11) to (6.14) a conjugate gradient algorithm for the iterative solution of problem (6.1). This derivation is straigthforward and left as an exercise.

7 Application to scattering problems

In this section we shall discuss an application of the methodology introduced in the above sections. It concerns the scattering of *monochromatic incident waves* by *purely reflecting* bodies (the case of *coated* obstacles is discussed in e.g. [6]).

7.1 Formulation of the scattering problems. Synopsis

Let us consider a scattering body B of boundary $\gamma = \partial B$, illuminated by an incident monochromatic wave. The scattered field satisfies (with $d = 2, 3$)

$$u_{tt} - \Delta u = 0 \quad in \quad (\mathbb{R}^d \backslash \bar{B}) \times (0, T), \tag{7.1}$$

$$u = g \quad on \quad \sigma = \gamma \times (0, T). \tag{7.2}$$

The unknown u represents for example the pressure for an acoustic problem or the non-zero component of the electric field satisfying the two-dimensional Maxwell's equations written in transverse magnetic (T.M.) form. The boundary condition (7.2) can be replaced by a Neumann one associated to a transverse electric (T.E.) formulation.

We have bounded $\mathbb{R}^d \backslash \bar{B}$ by an artificial boundary Γ and we denote by Ω the region of $\mathbb{R}^d$ between γ and Γ (see Figure 7.1); from now on we shall denote by Q the domain $\Omega \times (0,T)$.

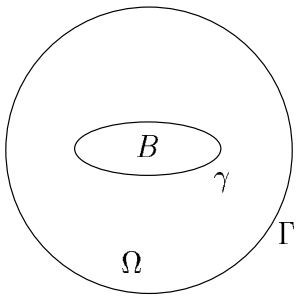

Figure 7.1:

We prescribe on Γ an *approximate Sommerfeld condition* such that

$$\frac{\partial u}{\partial n} + \frac{\partial u}{\partial t} = 0 \quad on \quad \Sigma = \Gamma \times (0,T). \tag{7.3}$$

The *first order* absorbing condition (7.3) can be replaced by a *second order* one (see, e.g., [9]) leading to better accuracy and efficiency.

Suppose that the harmonic wave hitting B is of period T ; we have then $g(x,t) = -Re(e^{-ikt}G(x))$ with $k = 2\pi/T$ and after some transition we shall reach a time-periodic regime of period T. From a computational point of view we have two classical possibilities :

With the *first one* we use a separation of variable method based on

$$u(x,t) = Re(e^{-ikt}U(x))$$

which leads to the following Helmholtz problem

$$\text{(7.4)} \qquad \begin{cases} \Delta U + k^2 U = 0 \quad in \quad \Omega, \\ U = G \quad on \quad \sigma, \\ \dfrac{\partial U}{\partial n} = ikU \quad on \quad \Gamma; \end{cases}$$

we shall not pursue in that direction (indeed the methods discussed in this section were developped precisely to solve problems such (7.4) by going back to the original problem (7.1)-(7.3)).

The second approach consists in time-integrating system (7.1)-(7.3) starting from initial conditions on u and u_t until a T-periodic regime has been reached. We shall follow this second approach; however since the asymptotic convergence as $t \to +\infty$ can be slow, particularly for *non-convex* reflectors, the idea is to speed it up using *control methods* like these discussed in Sections 1 to 6. Various numerical experiments have confirmed the soundness of our approach (see in particular the solution of the first test problem to be discussed later on in this article).

The methods of the above sections will be applied to system (7.1)-(7.3) completed by the following T-periodicity conditions

$$\text{(7.5)} \qquad u(0) = u(T), \quad u_t(0) = u_t(T).$$

7.2 Exact controllability and least-squares formulations

Solving problem (7.1)-(7.3), (7.5) is *equivalent* to finding a pair $\{e_o, e_1\}$ such that

$$\text{(7.6)} \qquad \begin{cases} u(0) = e_o, \quad u_t(0) = e_1, \\ u(T) = e_o, \quad u_t(T) = e_1, \end{cases}$$

with u solution of (7.1)-(7.3).

Problem (7.1)-(7.3), (7.6) is an *exact controllability problem* which can be solved by methods directly inspired from the J.L. Lions *Hilbert Uniqueness Method* (HUM) (see, e.g. [10], [11] and [5]), or from Section 1 to 6 after reformulating system (7.1)-(7.3), (7.5) in an equivalent first order in time form, such as

$$\text{(7.7)} \qquad \frac{\partial Z}{\partial t} + AZ = 0 \quad in \quad Q,$$

$$\begin{pmatrix} I & 0 \\ 0 & 0 \end{pmatrix} Z = \begin{pmatrix} g \\ 0 \end{pmatrix} \quad on \quad \sigma, \tag{7.8}$$

$$\begin{pmatrix} I & 0 \\ 0 & 0 \end{pmatrix} \frac{\partial Z}{\partial n} + \begin{pmatrix} 0 & I \\ 0 & 0 \end{pmatrix} Z = 0 \quad on \quad \Sigma, \tag{7.9}$$

$$Z(0) = Z(T), \tag{7.10}$$

with $Z = \begin{pmatrix} u \\ v \end{pmatrix}$ and $A = \begin{pmatrix} 0 & -I \\ -\Delta & 0 \end{pmatrix}$ (we have then $v = u_t$).

In order to avoid repeating Sections 1 to 6, we shall apply the controllability methodology directly on formulations (7.1)-(7.3), (7.5).

Back to (7.6), an appropriate choice for the space E containing $\{e_o, e_1\}$ is

$$E = V_g \times L^2(\Omega), \tag{7.11}$$

with $V_g = \{\varphi | \varphi \in H^1(\Omega), \varphi|\gamma = g(0)\}$. A *least-squares* formulation of (7.1)-(7.3), (7.6) is given by

$$\min_{v \in E} J_1(v), \tag{7.12}$$

with

$$J_1(v) = \frac{1}{2} \int_\Omega [|\nabla(y(T) - v_o)|^2 + |y_t(T) - v_1|^2] dx, \forall v = \{v_o, v_1\}, \tag{7.13}$$

where, in (7.13), the function y is *the* solution of

$$y_{tt} - \Delta y = 0 \quad in \quad Q, \tag{7.14}$$

$$y = g \quad on \quad \sigma, \tag{7.15}$$

$$\frac{\partial y}{\partial n} + \frac{\partial y}{\partial t} = 0 \quad on \quad \Sigma, \tag{7.16}$$

$$y(0) = v_o, \quad y_t(0) = v_1. \tag{7.17}$$

Remark 7.1 : The choice of J_1 as cost function is fairly natural once we realize that the *energy* $E(t)$ associated to the wave equation (7.14) is precisely

$$E(t) = \frac{1}{2}\int_\Omega [|\nabla y(t)|^2 + |y_t(t)|^2]dx.$$

Remark 7.2 : Functional J_1 leads to satisfactory computational results as shown in [3]-[6], [9] (and also in Section 7.6 of this article) ; however it has been shown in [8] that this functional may fail to be strongly "elliptic" (coercive) in some situations with *trapping rays*. As a cure, Bardos and Rauch have proposed in [8] the functional J_2, described just below, which has better coercivity properties than J_1. Functional J_2 is defined by

$$(7.18)\quad J_2(v) = \frac{1}{2}\int_Q [|\nabla(y(t) - Re(e^{-ikt}V(x)))|^2 + |y_t(t) - Re(-ike^{-ikt}V(x))|^2]dxdt,$$

with $V(x) = v_o(x) + iv_1(x)$ and y the solution of (7.14)-(7.17).

In Section 7.6, we shall compare the solutions obtained using functionals J_1 and J_2.

7.3 Gradient calculation. Optimality conditions

The solution of the least-squares problem (7.12) satisfies

$$(7.19)\qquad J_1'(e) = 0,$$

implying that computing $J_1'(v), \forall v \in E$ is a most important issue in itself. To address it, we proceed as in Section 4, using again a perturbation analysis. We have then (since $\delta v_o = 0$ on γ) :

$$(7.20)\qquad \delta J_1(v) = < J_1'(v), \delta v >,$$

and

$$(7.21)\qquad \left\{ \begin{array}{ll} \delta J_1(v) & = \displaystyle\int_\Omega \nabla(y(T) - v_o).\nabla\delta y(T)dx + \int_\Omega (y_t(T) - v_1)\delta y_t(T)dx \\ & + \displaystyle\int_\Omega \nabla(v_o - y(T)).\nabla\delta v_o dx + \int_\Omega (v_1 - y_t(T))\delta v_1 dx. \end{array} \right.$$

In (7.20), $< ., . >$ denotes the duality pairing between E_o' and E_o, where

$$(7.22)\qquad E_o = V_o \times L^2(\Omega) \text{ with } V_o = \{\varphi | \varphi \in H^1(\Omega), \varphi = 0 \text{ on } \gamma\}.$$

In (7.21), δy is solution of the following *perturbed wave system*

$$\delta y_{tt} - \Delta \delta y = 0 \quad in \quad Q, \tag{7.23}$$

$$\delta y = 0 \quad on \quad \sigma, \tag{7.24}$$

$$\frac{\partial \delta y}{\partial n} + \frac{\partial \delta y}{\partial t} = 0 \quad on \quad \Sigma, \tag{7.25}$$

$$\delta y(0) = \delta v_o, \delta y_t(0) = \delta v_1. \tag{7.26}$$

Introduce p a sufficiently smooth function of x and t satisfying

$$p(t) \in V_o, \forall t \in [0,T], \tag{7.27}$$

and therefore $p = 0$ on σ. Proceeding as in Section 1 and taking (7.23)-(7.27) into account we obtain by integration by parts and application of the divergence theorem that

$$\begin{aligned} 0 &= \int_Q p(\delta y_{tt} - \Delta \delta y) dx dt = \int_\Omega p(T) \delta y_t(T) dx - \int_\Omega p(0) \delta y_t(0) dx \\ &- \int_\Omega p_t(T) \delta y(T) dx + \int_\Omega p_t(0) \delta y(0) dx \\ &+ \int_Q (p_{tt} - \Delta p) \delta y dx dt + \int_\Sigma (\frac{\partial p}{\partial n} \delta y - p \frac{\partial \delta y}{\partial n}) d\Sigma \\ &+ \int_\sigma (\frac{\partial p}{\partial n} \delta y - p \frac{\partial \delta y}{\partial n}) d\sigma \end{aligned}$$

(with $d\Sigma = d\Gamma dt, d\sigma = d\gamma dt$), and then

$$\left\{ \begin{array}{ll} 0 &= \displaystyle\int_\Omega p(T) \delta y_t(T) dx - \int_\Omega p_t(T) \delta y(T) dx \\ &- \displaystyle\int_\Omega p(0) \delta v_1 dx + \int_\Omega p_t(0) \delta v_0 dx \\ &+ \displaystyle\int_Q (p_{tt} - \Delta p) \delta y dx dt \\ &+ \displaystyle\int_\Sigma (\frac{\partial p}{\partial n} \delta y + p \frac{\partial \delta y}{\partial t}) d\Sigma. \end{array} \right. \tag{7.28}$$

Suppose that function p satisfies

$$p_{tt} - \Delta p = 0 \quad in \quad Q; \tag{7.29}$$

relation (7.28) reduces, then, to

$$(7.30)\qquad \left\{ \begin{array}{l} \int_\Omega p(T)\delta y_t(T)dx - \int_\Omega p_t(T)\delta y(T)dx + \int_\Sigma (\frac{\partial p}{\partial n}\delta y + p\frac{\partial \delta y}{\partial t})d\Sigma = \\ \int_\Omega p(0)\delta v_1 dx - \int_\Omega p_t(0)\delta v_o dx. \end{array} \right.$$

By time integration by parts over Σ it follows from (7.30) that

$$(7.31)\qquad \left\{ \begin{array}{l} \int_\Omega p(T)\delta y_t(T)dx - \int_\Omega p_t(T)\delta y(T)dx + \int_\Gamma p(T)\delta y(T)d\Gamma \\ + \int_\Sigma (\frac{\partial p}{\partial n} - \frac{\partial p}{\partial t})\delta y d\Sigma = \int_\Omega p(0)\delta v_1 dx - \int_\Omega p_t(0)\delta v_o dx + \int_\Gamma p(0)\delta v_o d\Gamma. \end{array} \right.$$

Suppose that in addition to $p = 0$ on σ and (7.29), function p verifies also

$$(7.32)\qquad \frac{\partial p}{\partial n} - \frac{\partial p}{\partial t} = 0 \quad on \quad \Sigma,$$

$$(7.33)\qquad p(T) = y_t(T) - v_1$$

and

$$(7.34)\qquad \int_\Omega p_t(T)z dx = \int_\Gamma p(T)z d\Gamma - \int_\Omega \nabla(y(T) - v_o)\cdot\nabla z dx, \forall z \in V_o.$$

We have then, from (7.21), (7.31)-(7.34),

$$(7.35)\qquad \left\{ \begin{array}{l} < J_1'(v), w >= \int_\Omega \nabla(v_o - y(T))\cdot\nabla w_o dx + \int_\Gamma p(0)w_o d\Gamma \\ - \int_\Omega p_t(0)w_o dx + \int_\Omega (v_1 - y_t(T))w_1 dx + \int_\Omega p(0)w_1 dx, \\ \forall w = \{w_o, w_1\} \in E_o. \end{array} \right.$$

Remark 7.3 : Relations (7.34), (7.35) are largely formal; however, it is worth mentioning that the discrete variants of the above two relations make sense and lead to algorithms with fast convergence properties (in order to make (7.34) rigorous we should replace the integral in the left-hand side of the above equation by a duality pairing; similarly, we should replace the boundary integral in the right-hand side of (7.34) by a well-chosen duality pairing).

7.4 Conjugate Gradient Solution of the Least-Squares Problem (7.12)

A conjugate gradient algorithm for the solution of problem (7.12) will be described below; it is closely related to algorithm (5.1)-(5.13), from Section 5 and is as follows :

Step 0 : Initialization

$$e^o = \{e_o^o, e_1^o\} \in E \text{ is given.} \tag{7.36}$$

Solve the following forward wave problem

$$y_{tt}^o - \Delta y^o = 0 \quad in \quad Q, \tag{7.37}_1$$

$$y^o = g \quad on \quad \sigma, \tag{7.37}_2$$

$$\frac{\partial y^o}{\partial n} + \frac{\partial y^o}{\partial t} = 0 \quad on \quad \Sigma, \tag{7.37}_3$$

$$y^o(0) = e_o^o, y_t^o(0) = e_1^o. \tag{7.37}_4$$

Solve the following backward wave problem

$$p_{tt}^o - \Delta p^o = 0 \quad in \quad Q, \tag{7.38}_1$$

$$p^o = 0 \quad on \quad \sigma, \tag{7.38}_2$$

$$\frac{\partial p^o}{\partial n} - \frac{\partial p^o}{\partial t} = 0 \quad on \quad \Sigma, \tag{7.38}_3$$

with $p^o(T)$ *and* $p_t^o(T)$ *given by*

$$p^o(T) = y_t^o(T) - e_1^o, \tag{7.38}_4$$

$$\int_\Omega p_t^o(T) z dx = \int_\Gamma p^o(T) z d\Gamma - \int_\Omega \nabla(y^o(T) - e_o^o) \cdot \nabla z dx, \forall z \in V_o, \tag{7.38}_5$$

respectively.

Define next $g^o = \{g_o^o, g_1^o\} \in E_o = V_o \times L^2(\Omega)$ *by*

$$(7.39)_1 \qquad \begin{cases} \displaystyle\int_\Omega \nabla g_o^o \cdot \nabla z dx = \int_\Omega \nabla(e_o^o - y^o(T)) \cdot \nabla z dx \\ \displaystyle -\int_\Omega p_t^o(0) z dx + \int_\Gamma p^o(0) z d\Gamma, \forall z \in V_o, \end{cases}$$

$$(7.39)_2 \qquad g_1^o = p^o(0) + e_1^o - y_1^o(T),$$

and then

$$(7.40) \qquad w^o = g^o. \blacksquare$$

For $k \geq 0$, *suppose that* e^k, g^k, w^k *are known ; we compute then their updates* $e^{k+1}, g^{k+1}, w^{k+1}$ *as follows*

Step 1 : Descent

Solve

$$(7.41)_1 \qquad \bar{y}_{tt}^k - \Delta \bar{y}^k = 0 \quad in \quad Q,$$

$$(7.41)_2 \qquad \bar{y}^k = 0 \quad on \quad \sigma,$$

$$(7.41)_3 \qquad \frac{\partial \bar{y}^k}{\partial n} + \frac{\partial \bar{y}^k}{\partial t} = 0 \quad on \quad \Sigma,$$

$$(7.41)_4 \qquad \bar{y}^k(0) = w_o^k, \bar{y}_t^k(0) = w_1^k.$$

Solve the following backward wave problem

$$(7.42)_1 \qquad \bar{p}_{tt}^k - \Delta \bar{p}^k = 0 \quad in \quad Q,$$

$$(7.42)_2 \qquad \bar{p}^k = 0 \quad on \quad \sigma,$$

$$(7.42)_3 \qquad \frac{\partial \bar{p}^k}{\partial n} - \frac{\partial \bar{p}^k}{\partial t} = 0 \quad on \quad \Sigma,$$

with $\bar{p}^k(T)$ *and* $\bar{p}^k_t(T)$ *given by*

$$\bar{p}^k(T) = \bar{y}^k_t(T) - w^k_1, \tag{7.42}_4$$

$$\int_\Omega \bar{p}^k_t(T) z dx = \int_\Gamma \bar{p}^k(T) z d\Gamma - \int_\Omega \nabla(\bar{y}^k(T) - w^k_o) \cdot \nabla z dx, \forall z \in V_o, \tag{7.42}_5$$

respectively.

Define next $\bar{g}^k = \{\bar{g}^k_o, \bar{g}^k_1\} \in V_o \times L^2(\Omega)$ *by*

$$\left\{ \begin{array}{l} \displaystyle\int_\Omega \nabla \bar{g}^k_o \cdot \nabla z dx = \int_\Omega \nabla(w^k_o - \bar{y}^k(T)) \cdot \nabla z dx \\ \displaystyle - \int_\Omega \bar{p}^k_t(0) z dx + \int_\Gamma \bar{p}^k(0) z d\Gamma, \forall z \in V_o, \end{array} \right. \tag{7.43}_1$$

$$\bar{g}^k_1 = \bar{p}^k(0) + w^k_1 - \bar{y}^k_t(T), \tag{7.43}_2$$

and then ρ_k *by*

$$\rho_k = \frac{\int_\Omega [|\nabla g^k_o|^2 + |g^k_1|^2] dx}{\int_\Omega (\nabla \bar{g}^k_o \cdot \nabla w^k_o + \bar{g}^k_1 w^k_1) dx}. \tag{7.44}$$

We update then e^k *and* g^k *by*

$$e^{k+1} = e^k - \rho_k w^k, \tag{7.45}$$

$$g^{k+1} = g^k - \rho_k \bar{g}^k. \tag{7.46}$$

Step 2 : Test of the convergence and construction of the new descent direction

If

$$\frac{(\int_\Omega (|\nabla g^{k+1}_o|^2 + |g^{k+1}_1|^2) dx)^{1/2}}{(\int_\Omega (|\nabla g^o_o|^2 + |g^o_1|^2) dx)^{1/2}} \leq \varepsilon$$

take $e = e^{k+1}$ *; else, compute*

$$\gamma_k = \frac{\int_\Omega ((|\nabla g^{k+1}_o|^2 + |g^{k+1}_1|^2) dx}{(\int_\Omega (|\nabla g^k_o|^2 + |g^k_1|^2) dx} \tag{7.47}$$

and update w^k *by*

$$w^{k+1} = g^{k+1} + \gamma_k w^k. \blacksquare \tag{7.48}$$

Do $k = k + 1$ *and go to* (7.41).

Remark 7.4 : Algorithm (7.36)-(7.48) looks complicated at first glance. In fact, it is not that complicated to implement since each iteration requires basically the solution of two wave equations such as (7.41) and (7.42) and of an elliptic problem such as $(7.43)_1$. The above problems are classical ones for which efficient solution methods already exist.

Remark 7.5 : Remark 5.3 still holds for algorithm (7.36)-(7.48).

7.5 Space-time discretization

The practical implementation of the above control based computational method is straightforward in the sense that it relies on fairly classical finite difference time discretization schemes and finite element approximations. To be more precise the basic wave problem

$$u_{tt} - \Delta u = 0 \quad in \quad Q, \tag{7.49}_1$$

$$u = g \quad on \quad \sigma, \tag{7.49}_2$$

$$\frac{\partial u}{\partial n} + \frac{\partial u}{\partial t} = 0 \quad on \quad \Sigma, \tag{7.49}_3$$

$$u(0) = u_o, u_t(0) = u_1, \tag{7.49}_4$$

will be approximated as follows :

Step 1 : We introduce the following *variational formulation* of problem (7.49) :

$$\left\{ \begin{array}{l} \textit{Find } u \textit{ satisfying } u(t) \in H^1(\Omega), \forall t \in [0,T], \textit{ and} \\ \displaystyle\int_\Omega u_{tt} z dx + \int_\Omega \nabla u \cdot \nabla z dx + \int_\Gamma \frac{\partial u}{\partial t} z d\Gamma = 0, \forall z \in V_o, \textit{ a.e. on } (0,T), \end{array} \right. \tag{7.50}$$

relation (7.50) being completed by $(7.49)_2, (7.49)_4$. The space V_o is still defined by (7.22).

Step 2 : As in Section 6, we introduce $\Delta t = T/N$; we then (formally) *time discretize* $(7.49)_2, (7.49)_4, (7.50)$ by

$$(7.51)_1 \qquad u^o = u_o, \quad u^1 - u^{-1} = 2\Delta t u_1,$$

and for $n = 0, 1, \ldots, N$, we compute u^{n+1} via the solution of

$$(7.51)_2 \qquad \left\{ \begin{array}{l} u^{n+1} \in V_{g^{n+1}}; \forall z \in V_o \text{ we have} \\ \\ \displaystyle\int_\Omega \frac{u^{n+1} + u^{n-1} - 2u^n}{\Delta t^2} z dx + \int_\Omega \nabla u^n \cdot \nabla z dx \\ \displaystyle + \int_\Gamma \frac{u^{n+1} - u^{n-1}}{2\Delta t} z d\Gamma = 0, \end{array} \right.$$

with

$$V_{g^{n+1}} = \{z | z \in H^1(\Omega), z = g((n+1)\Delta t) \text{ on } \gamma\}.$$

Scheme (7.51) is (formally) *second order accurate* with respect to Δt.

Step 3 : We suppose -for simplicity- that Ω is a *bounded polygonal* domain of $\mathbb{R}^2$. With $\mathcal{T}_h$ a classical *finite element triangulation* of Ω, we approximate $H^1(\Omega)$ and $L^2(\Omega)$ by

$$(7.52) \qquad V_h = \{z | z \in C^o(\bar{\Omega}), z|_T \in P_1, \forall T \in \mathcal{T}_h\},$$

where P_1 is the space of polynomials in two variables of degree ≤ 1, and where -as usual- h is the length of the largest edge(s) of $\mathcal{T}_h$. With obvious notation, we approximate (7.49) by

$$(7.53)_1 \qquad u_h^o = u_{oh}, \quad u_h^1 - u_h^{-1} = 2\Delta t u_{1h},$$

and, for $n = 0, 1, \ldots, N$, by

$$(7.53)_2 \qquad \left\{ \begin{array}{l} u_h^{n+1} \in V_{g_h^{n+1}}, \\ \\ \displaystyle\int_\Omega \frac{u_h^{n+1} + u_h^{n-1} - 2u_h^n}{\Delta t^2} z dx + \int_\Omega \nabla u_h^n \cdot \nabla z dx \\ \displaystyle + \int_\Gamma \frac{u_h^{n+1} - u_h^{n-1}}{2\Delta t} z d\Gamma = 0, \forall z \in V_{oh}, \end{array} \right.$$

where, in (7.53), u_{oh} and u_{1h} are approximations of u_o and u_1 belonging to V_h and where

$$V_{oh} = \{z | z \in V_h, z = 0 \ on \ \gamma\} (= V_o \cap V_h),$$
$$V_{g_h^{n+1}} = \{z | z \in V_h, z = g_h^{n+1} \ on \ \gamma\},$$

g_h^{n+1} being an approximation of $g((n+1)\Delta t)$ belonging to the boundary space span by the traces on γ of the functions of V_h.

Scheme (7.53) is *conditionally stable* only and Δt has to satisfy a *stability condition* such as

$$\Delta t < C \ h \tag{7.54}$$

where, in (7.54), C is a constant (for a wave equation like the one in (7.49), it is strongly advised to use triangulations with small aspect ratio, i.e. $h/h_{min} \approx 1$, with h_{min} the length of the smallest edge(s) of $\mathcal{T}_h$). If (7.54) holds and if the data u_o, u_1 and g are sufficiently smooth, scheme (7.53) is second order accurate with respect to h and Δt. Since the wave equation (7.49) is a model for waves propagating with velocity 1 a condition such as (7.54) is not very limitative in practice.

Actually, obtaining u_h^{n+1} from u_h^{n-1} and u_h^n requires the solution of a linear system in $\mathbb{R}^{N_{oh}}$ where $N_{oh} = dim(V_{oh})$. To obtain this linear system we expand u_h^{n+1} over a vector basis of V_h, then take the boundary conditions into account and, finally, take for z in $(7.53)_2$ the vectors of a basis of V_{oh}. The resulting matrix is symmetric and positive definite but *not diagonal*. Actually if instead of computing exactly the integrals such as $\int_\Omega u_h^{n+1} z dx$, we approximate them, using the two-dimensional trapezoidal rule, we obtain a linear system with a $N_{oh} \times N_{oh}$ *diagonal* matrix whose diagonal entries are strictly positive. The above operation is called *mass lumping* and implies some accuracy loss particularly for non structured triangulations $\mathcal{T}_h$. Let us mention however that for scattering problems we systematically try to use meshes as structured as possible.

To compute u_h^{n+1} in (7.53), the more expensive part is the computation of the matrix-vector product corresponding to the evaluation of the term $\int_\Omega \nabla u_h^n \cdot \nabla z dx$; on the other hand, if an iterative algorithm is used to compute the solution of the linear systems $(7.39)_1$ and $(7.43)_1$, the main cost of this preconditioning step is also related to the same matrix-vector product. So, for the efficiency of the global algorithm, the matrix-vector product has to be as optimized as possible. The matrix being sparse and symmetric, only the non-zero terms of the lower triangular matrix are stored. If the computations are done on a vector machine, as we intend here, we need

vectorizable algoritms. If we consider a line storage, the vectors are short and the vectorization not very efficient. That's why we have considered a diagonal storage (see [12]) for the non-zero terms, the length of the vectors is then the number of non-zero terms of the diagonals. To optimize this length, a renumbering algorithm minimizing the matrix bandwidth is previously applied.

7.6 Numerical Experiments

7.6.1 Generalities

In the following paragraphs we are going to discuss the application of the above computational methods to the solution of two and three dimensional scattering problems for *perfectly conducting* obstacles of various shapes.

To obtain accurate solutions one needs to have h at least *ten times smaller* than the wavelength λ, and, indeed, the local space discretization step has to be even smaller (of the order of $\lambda/20$) in those regions with internal rays trapped by successive reflections. For the mesh generation we have used an advancing front method, for the 2-D meshes see [13], for the 3-D ones see [14],[15]. This method gives good quality meshes implying that we can choose a reasonable time step satisfying nevertheless the CFL condition (7.54).

The discrete elliptic problems associated to the preconditioning steps $(7.43)_1$, have been solved by either a direct method "à la Cholesky" if the matrix is not too large or a conjugate gradient. If a direct method is used, the matrix is factorized once for all. If a conjugate gradient is used, as we have to solve successively linear systems with the same matrix and different right hand sides, we can use an augmented conjugate gradient to improve the convergence (see [16],[17]).

Concerning the location of the artificial boundary we have used the following strategy for the 2-D cases : if (7.3) is used, then one takes the artificial boundary Γ at a distance 3λ to ∂B ; if, on the other hand, one uses the second order absorbing boundary condition described in [9, Section 3], one takes Γ at a distance λ to ∂B. For the 3-D test cases, one locates the artificial boundary at a distance λ to ∂B and uses only the first order boundary condition.

To conclude these generalities on the numerical experiments, let us mention the importance of properly choosing e_o^o and e_1^o in algorithm (7.36)-(7.48). In order to define smooth initial conditions satisfying the boundary conditions on the obstacle, we can solve, for example, a Poisson equation. Another possibility, leading to a faster convergence to the harmonic solution, is to prescribe the time harmonic sources progressively during a transient time interval $[0, t_{tr}]$ as suggested by G. Mur [18].

On this time interval, the function g in (7.2) is multiplied by a smooth transition function θ_{tr} increasing from 0 to 1 ; we have used the function θ_{tr} suggested in [18], namely

$$(7.55) \qquad \begin{cases} \theta_{tr}(t) = (2 - \sin((t/t_{tr})\frac{\pi}{2}))\sin((t/t_{tr})\frac{\pi}{2}), \ if \ \ 0 < t \leq t_{tr}, \\ \theta_{tr}(t) = 1, \ if \ \ t \geq t_{tr}. \end{cases}$$

For simple convex obstacles, we obtain generally at t_{tr} the harmonic solution ; for non convex obstacles, we apply for $t \geq t_{tr}$, the control algorithm to reach complete convergence as shown in the numerical results.

7.6.2 2-D numerical results

The first 2-D case concerns a perfectly conducting circular cavity with an open crack, and we consider the transverse electric (T.E.) problem. If we denote by a the external diameter of the cavity, the thickness of the wall is 0.025 a and the height of the crack is also 0.025 a. The wavelength of the incident wave is 0.3 a. The mesh has 45,527 nodes and 89,861 triangles. An enlargment of the mesh near the crack is shown in Figure 7.2. If we denote by h_m the mean length of the triangle edges, we have $h_m \simeq \lambda/40$ inside the cavity and $h_m = \lambda/20$ outside. One can observe the regularity of the mesh obtained by the advancing front method. For this case we use the first order absorbing boundary condition and the artificial boundary Γ is located at a distance to the cavity of 3λ. The time step is $T/72$.

Figure 7.3 shows the scattered field (e_o or real part) for an incident wave coming from the left. On Figures 7.4-7.6, we compare the convergence histories of the residuals with three different approaches :

Fig.7.4: integration in time without control,

Fig.7.5: control algorithm with functional J_1 defined by (7.13),

Fig.7.6: control algorithm with functional J_2 defined by (7.18).

The continuous curves represent the residuals defined by

$$Res_o = \frac{[\int_\Omega |e_o^{k+1} - e_o^k|^2 dx]^{\frac{1}{2}}}{[\int_\Omega |e_o^1 - e_o^o|^2 dx]^{\frac{1}{2}}},$$

with e_o^k denoting either the solution after k periods for Figure 7.4 , or the solution of the kth iteration of the conjugate gradient algorithm for Figures 7.5 and 7.6. The dotted lines represent the residuals associated to e_1. The solution obtained by

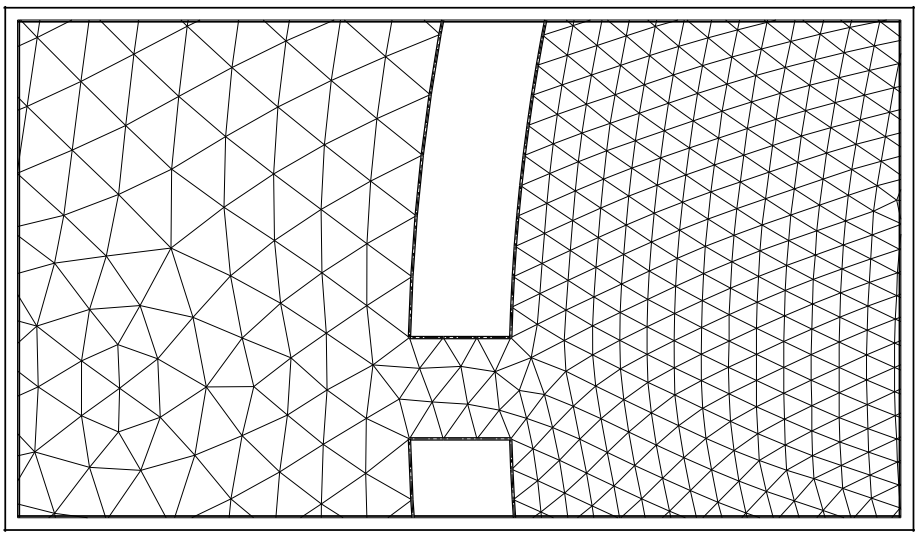

Figure 7.2: Circular cavity: enlargment of the mesh near the crack.

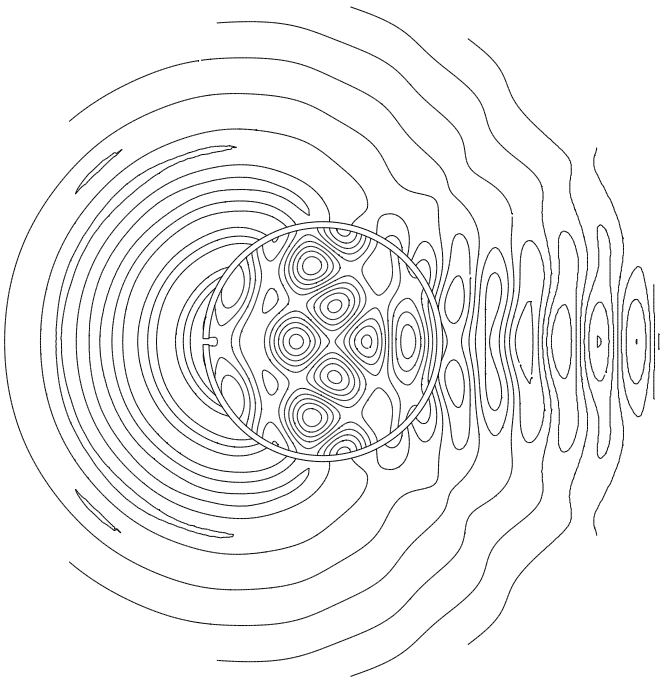

 Figure 7.3: Circular cavity: scattered field (e_o).

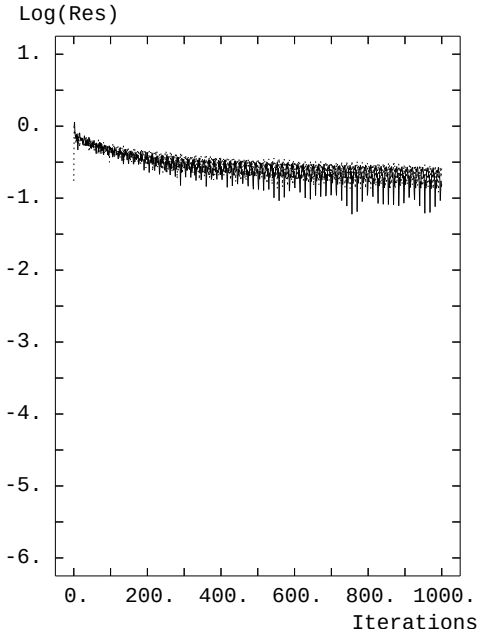

Figure 7.4: Residual convergence history.Integration in time without control.

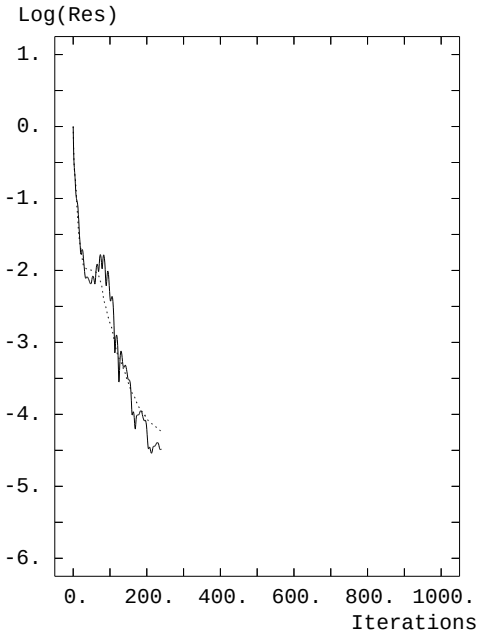

Figure 7.5: Residual convergence history.Control with cost function J_1.

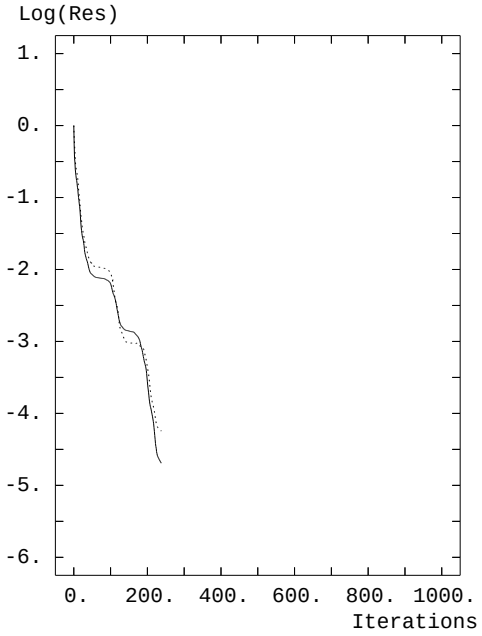

Figure 7.6: Residual convergence history.Control with cost function J_2.

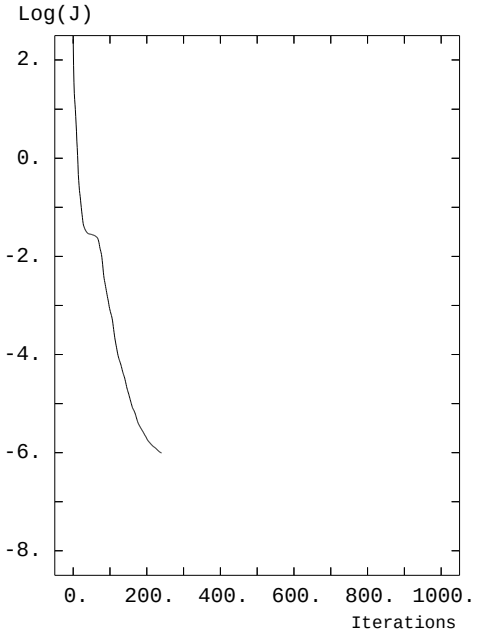

Figure 7.7: Cost function J_1 convergence history.

only the integration in time is not converged ; the solutions obtained by the two control approaches are the same, but we can observe that the convergence related to $e_o(Res_o)$ is monotone in Fig. 7.6 associated to J_2, but not in Fig. 7.5 associated to J_1. Of course, the decays of the cost functions J_1 or J_2 are monotone (see Fig. 7.7). The computed solutions being the same and the approach with J_1 being less memory consuming, the following examples have been computed by control via the functional J_1.

The second 2-D case concerns the scattering by a semi-open rectangular cavity; the internal dimensions of the cavity are $20\lambda \times 5\lambda$ and the thickness of the wall is λ as shown in Figure 7.8. The artificial boundary is located at one wavelength to the cavity and we use the second order boundary condition. The triangulation contains 136,228 nodes and 268,776 triangles, we have $h_m \simeq \lambda/30$ inside the cavity and $h_m \simeq \lambda/20$ outside. The time step is $T/60$. We consider an illuminating wave of incidence $-30°$. Figure 7.9 shows the total field for the transverse magnetic (T.M.)

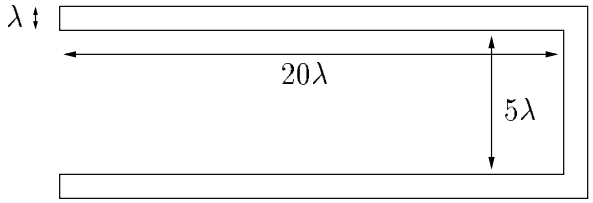

Figure 7.8: Semi-open rectangular cavity

mode, while in Figure 7.10 we have visualized the corresponding R.C.S. plotted in polar coordinates.

7.6.3 3-D numerical results

We consider now 3-D acoustic problems ; the first geometry is a 3-D semi-open cylindrical cavity ; the internal radius is 0.5λ, the length of the cavity is 2λ and the wall thickness is 0.1λ. The mesh has about 220,000 nodes and 1,235,000 tetrahedra with $h_m \simeq \lambda/25$ inside the cavity and $h_m \simeq \lambda/15$ outside. Figure 7.11 shows the trace of the mesh on the cavity. We use as time step $\Delta t = T/70$. With the angles defined as in Fig.7.12, the incident wave is defined by $\theta = 150°, \varphi = 0°$.

With $t_{tr} = 10T$, the convergence is reached after 20 conjugate gradient iterations and a global CPU time of 440 s on Cray C90. In Figure 7.13, the contours of the scattered field (e_o) are shown in the cross section by the plane $(z = 0)$. The RCS in

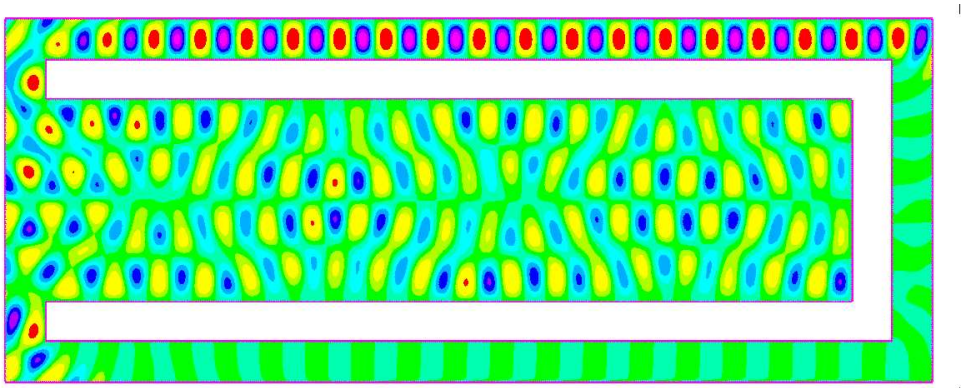

Figure 7.9: Rectangular cavity: total field.

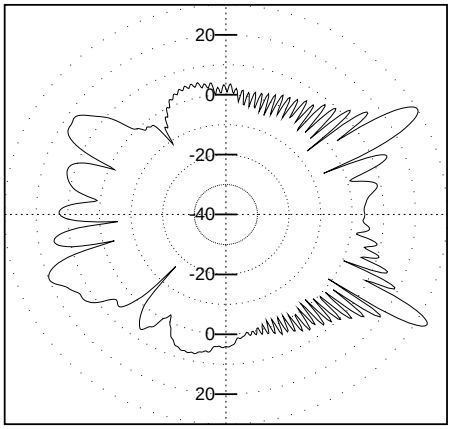

Figure 7.10: Rectangular cavity: RCS

the same plane is shown in Figure 7.14. Figure 7.15 shows the convergence history of the cost function J_1.

These three first examples were test cases of the Oxford Workshop ; the results presented here are in good agreement with the results obtained by different other methods (see [19]).

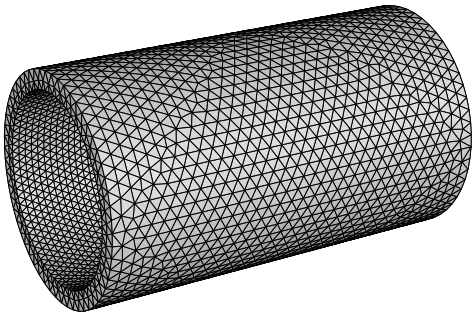

Figure 7.11: Trace of the mesh on the boundary of the cylindrical semi-open cavity.

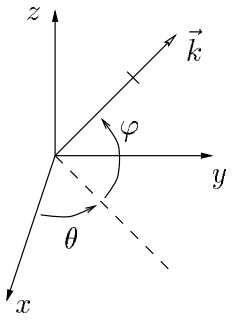

Figure 7.12: Definition of the angles.

Another 3-D acoustic example concerns an idealized air-intake as shown in Figure 7.16, the artificial boundary is a circular cylinder located, at least, at one wavelength of the obstacle. The characteristic length of the air-intake is 4 wavelengths. The mesh has about 327,000 nodes and 1,832,000 tetrahedra. We use as time step $\Delta t = T/70$. With the angles defined as in Fig. 7.12, the incident wave is defined by $\theta = 90°, \varphi = 45°$.

With $t_{tr} = 10T$, the convergence is reached after 20 conjugate gradient iterations and a CPU time of 12 mn on Cray C90. In Figure 7.17 we have visualized the scattered field in the cross section by the plane ($x = 0$). The RCS in the same plane is shown in Figure 7.18.

8 Further Comments and Conclusion

In this article, we have discussed a *least-squares/shooting method* for the numerical calculation of the time-periodic solutions of some linear dynamical systems and we have applied these techniques to the simulation of *scattering phenomena* where planar harmonic waves hit *non-convex* obstacles. This approach, which relies on *control* techniques, provides an efficient and easy to implement alternative to more classical *Helmholtz equation* solvers, like those discussed in, e.g. [20] (see also the references therein). It has also the advantage of being applicable, even if the forcing terms are T-periodic, non-harmonic, i.e. not of the form $A(x)\cos 2\pi t/T + B(x)\sin 2\pi t/T$. The

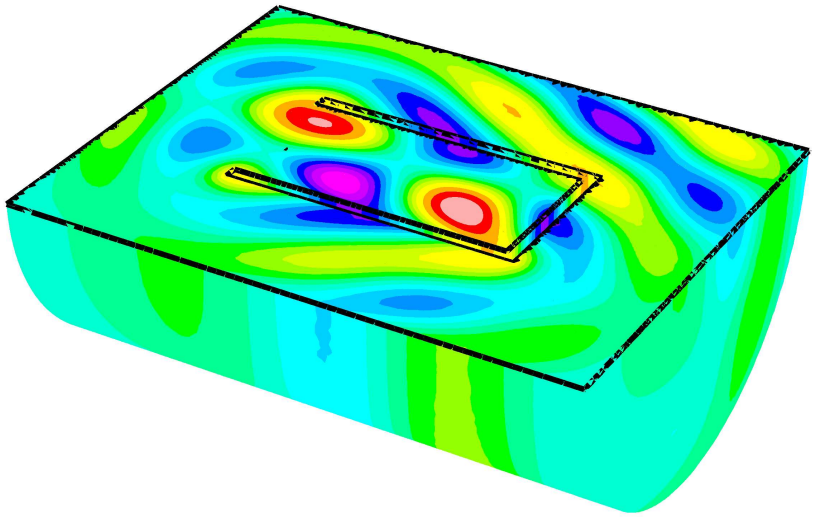

Figure 7.13: Cylindrical cavity: contours of the scattered field in a cross-section

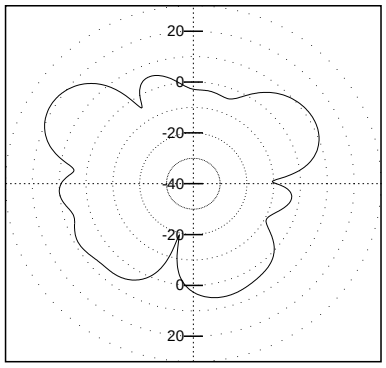

Figure 7.14: Cylindrical cavity: RCS in the incidence plane.

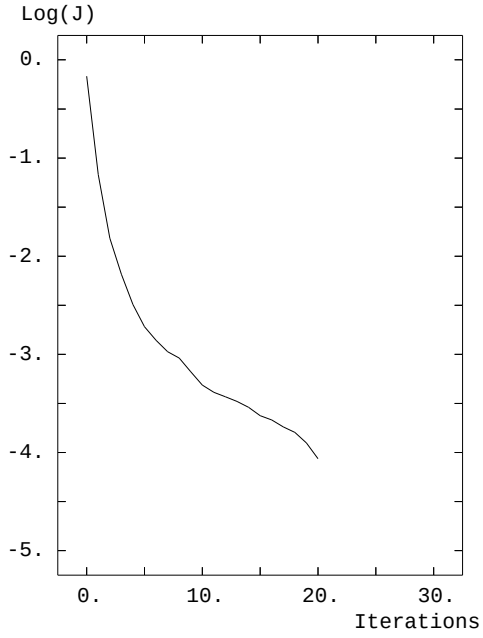

Figure 7.15: Cost function J_1 convergence history.

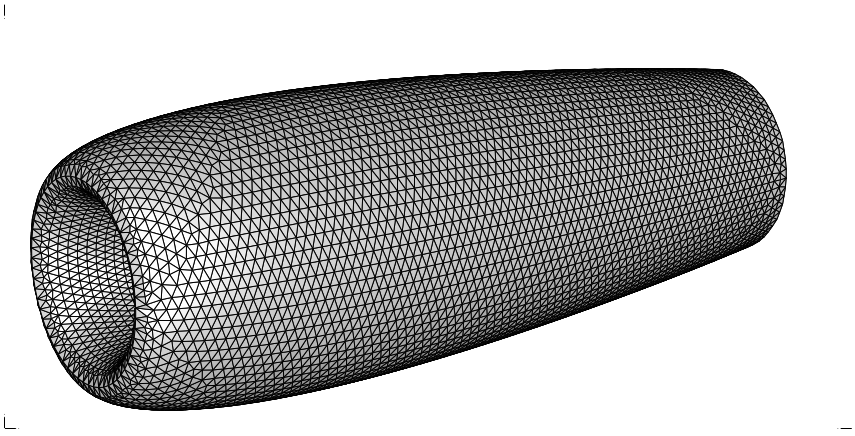

Figure 7.16: Trace of the mesh on the air-intake boundary.

methodology discussed in this article has been applied, in [21], to the solution of three dimensional scattering problems for *Electro-Magnetic Waves* modeled by the *Maxwell Equations*. Actually, these least-squares/shooting methods can also be applied to the calculation of the T-periodic solutions of *nonlinear partial differential equations*. Computing the gradient of the least-squares objective function requires the *backward integration* from $t = T$ to $t = 0$ of an adjoint equation, *linear*, but with time dependent coefficients since they are functions of the (known) solution of the state equation, i.e. the solution of the non-linear analog of (3.3). The *dynamical memory saving* technique described in [22], allows to avoid recording the solution of the state equation at all the time discretization steps and makes indeed the storage requirements of the above least-squares/shooting method very reasonable (see [22] for the details of this method).

Acknowledgments : The authors would like to thank C. Bardos, J. Erhel, J.L. Lions and B. Mantel for helpful comments and suggestions. The work described here was partially suggested by DRET, NSF, DARPA and the Texas Higher Education Coordinating Board.

A part of the computations have been done on the Cray C98 of IDRIS, France.

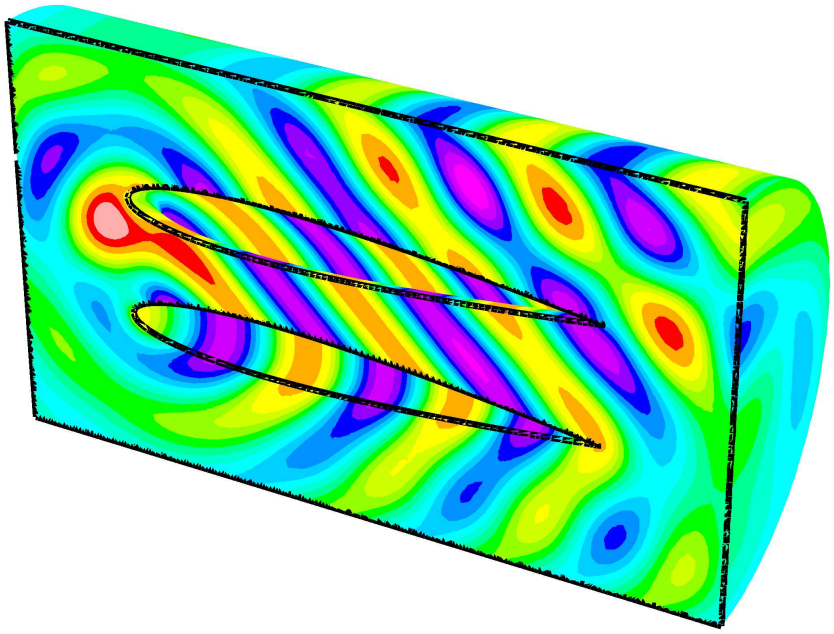

Figure 7.17: Air-intake: contours of the scattered field.

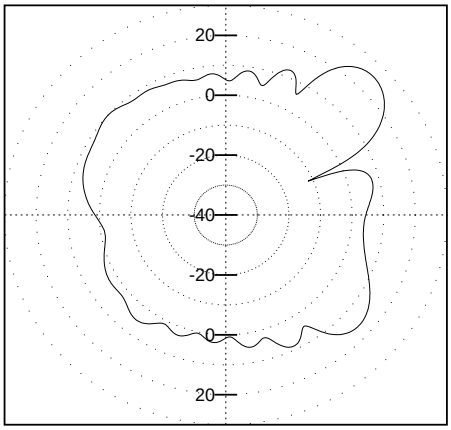

Figure 7.18: Air-intake: RCS in the incidence plane.

A Computation of the Radar Cross Section

In this section, we give some details on the computation of the radar cross section of a scatterer, on its numerical approximation and finally some numerical results are discussed.

A.1 Definition of the RCS

With the assumption of Sec. 7.1 ($g(x,t) = Re(e^{-ikt}G(x))$), we will use the complex form of the solution, i.e.

$$U(x) = u(x,0) + \frac{i}{k}\frac{\partial u}{\partial t}(x,0). \tag{A.1}$$

In spherical polar coordinates (r,θ,φ), the scattering cross section or bistatic radar cross section $\sigma(\theta,\varphi)$ is defined by (see [23]):

$$\sigma(\varphi) = \lim_{r\to\infty} 2\pi r \frac{|U(r,\varphi)|^2}{|U^{inc}(r,\varphi)|^2} \quad if \quad d=2, \tag{A.2}$$

and

$$\sigma(\theta,\varphi) = \lim_{r\to\infty} 4\pi r^2 \frac{|U(r,\varphi,\theta)|^2}{|U^{inc}(r,\varphi,\theta)|^2} \quad if \quad d=3. \tag{A.3}$$

In the following, by generalization, we will use the expression "Radar Cross Section" (RCS) for electromagnetic or acoustic cases.

Thus, to compute the RCS, we need far field scattering data. For this, we use the usual near field to far field transformation (see [23], [24]), allowing to compute the value of the scattered field at any point outside of an arbitrary surface C which completely encloses the obstacle, if the solution and its normal derivative are known on this surface C. This transformation uses the Green function (elementary solution of Helmholtz equation).

For any point $M(r,\varphi)$, (resp., $M(r,\theta,\varphi)$), we define the unit vector e_r by

$$e_r = \begin{pmatrix} \cos\varphi \\ \sin\varphi \end{pmatrix}, \quad (\text{resp., } e_r = \begin{pmatrix} \cos\theta\cos\varphi \\ \sin\theta\cos\varphi \\ \sin\varphi \end{pmatrix}). \tag{A.4}$$

Then after using the near field to far field transformation and the limit behaviour for $r \to \infty$, we obtain (assuming that $|U^{inc}| = 1$):
if $d = 2$,

$$\sigma(\varphi) = \frac{4}{k}|P(\varphi)|^2 \tag{A.5}$$

with

$$P(\varphi) = -\frac{i}{4}\int_C (\frac{\partial U}{\partial n} + ik(n.e_r)U)e^{-ikr'e_{r'}.e_r}ds, \tag{A.6}$$

and, if $d = 3$

$$\sigma(\theta,\varphi) = \frac{4\pi}{k^2}|S(\theta,\varphi)|^2, \tag{A.7}$$

with

$$S(\theta,\varphi) = -\frac{k}{4\pi}\int_C (\frac{\partial U}{\partial n} + ik(n.e_r)U)e^{-ikr'e_{r'}.e_r}ds, \tag{A.8}$$

where $M'(r',\varphi')$ (resp., $M'(r',\theta',\varphi')$) is a point on C and n is the unit outward normal at C at this point.

In the following figures, we will show the quantity RCS defined by

$$\text{RCS} = 10log_{10}(\frac{\sigma}{\lambda}) \quad if \quad d = 2, \tag{A.9}$$

$$\text{RCS} = 10log_{10}(\frac{\sigma}{\lambda^2}) \quad if \quad d = 3. \tag{A.10}$$

A.2 Numerical approximation

In the following, we choose as surface C, the surface of the obstacle; the artificial boundary Γ could also be used (see remark A.1). Since we use unstructured meshes, it would be necessary to use some domain decomposition technique to define another regular surface included in the computational domain.

We assume that the solution is discretized as proposed in Sec. 7.5, so it is defined at each node of the mesh; to compute σ from (A.5)-(A.8) the difficulty is to define an accurate approximation of the normal derivative $\frac{\partial U}{\partial n}$. In the following we introduce and compare three numerical approximations of this term ; these approximations are written here only for the 3-D cases, but defining the 2-D analogs is as easy.

If we denote by $\mathcal{T}_h$ a finite element tetrahedrisation of Ω, let S_h be the set of the faces S belonging to γ and M_h the set of the nodes belonging to γ.

The solution U_h being piecewise linear, the simplest way to define a normal derivative is to define $\frac{\partial_h U_h}{\partial n}$ as a constant on each face S of the obstacle boundary by:

$$\frac{\partial_h U_h}{\partial n}|_S = \nabla u_h|_S \cdot n_S, \forall S \in S_h \tag{A.11}$$

where n_S denotes the unit outward normal to the face S.

An other possibility is to consider $\frac{\partial_h U_h}{\partial n}$ as piecewise linear with its value at each node defined by a weighted average :

$$\nabla_h U_h|_i = \frac{1}{V_i} \sum_{T \in B_i} V(T) \nabla U_h|_T, \tag{A.12}$$

and

$$\frac{\partial_h U_h}{\partial n}|_i = \nabla_h U_h|_i \cdot n_i, \forall M_i \in M_h, \tag{A.13}$$

with

B_i the set of the tetrahedra T such as $M_i \in T$,
$V(T)$ the volume of the tetrahedron T,
V_i the sum of the volumes of the tetrahedra belonging to B_i,
n_i the unit outward normal defined at the node M_i by averaging.

To define a third approximation of $\frac{\partial U}{\partial n}$, we can use Green's formula and the fact that the solution U_h is an approximate solution of Helmholtz equation. From Green's formula, we have

$$\int_\gamma \frac{\partial U_h}{\partial n} z_i d\gamma = \int_\Omega \Delta U_h z_i dx + \int_\Omega \nabla U_h \cdot \nabla z_i dx, \tag{A.14}$$

with z_i the basis function associated to the node $M_i \in M_h$.

The solution U_h being an approximate solution of the Helmholtz equation (7.4), we can replace ΔU_h by $-k^2 U_h$. We define then a new piecewise linear approximation $\frac{\partial_h U_h}{\partial n}$ by :

$$\frac{\partial_h U_h}{\partial n}|_i = \frac{3}{A_i}[\int_{B_i} \nabla U_h \cdot \nabla z_i dx - k^2 \int_{B_i} U_h z_i dx], \forall M_i \in M_h \tag{A.15}$$

with A_i the sum of the areas of the faces S such as $M_i \in S$.

We have used a mass lumping formula to compute the left hand side of (A.14) and obtain (A.15); the two integrals of the right hand side of (A.15) can be computed exactly.

Once an approximation of $\frac{\partial U}{\partial n}$ is defined, we can compute the discrete integrals of (A.5), (A.7) using a numerical integration procedure; the term $e^{-ikr' e_{r'} . e_r}$ is considered as linear for the integration.

Remark A.1 *We could also consider as surface C the artificial boundary Γ and use the radiation condition (7.3) to define $\frac{\partial U}{\partial n}$ (or even a second order one, see [9]). The corresponding numerical results have not been very accurate, therefore this approximation is not detailed here.*

A.3 Numerical experiments

In this part, we compare the accuracy of the different approximations by computing on simple geometries, on one hand the exact RCS and on the other hand the RCS of the exact solution, so that we can estimate the accuracy of the RCS computation in itself. Finally the RCS of a computed solution is also compared. Of course the control approach is not necessary to compute the solution on these simple obstacles (cylinder and sphere), but these geometries are considered to validate the RCS computations, analytical solutions being available. The exact solution and RCS are computed using Bessel functions (see [23])

A.3.1 2-D Numerical experiments

For the 2-D comparisons, we consider a circular cylinder of radius $r = 2\lambda$. The artificial boundary is located at a distance λ to ∂B. For the computed solution and RCS, the mesh consists of 4,248 nodes and 8,024 triangles. For the computed solution, we use a second-order absorbing boundary condition (see [9]).

The RCS are computed each half degree.

In Figure A.1, (resp., A.2, A.3), we compare the exact RCS (dotted line) with the exact solution's computed RCS (continuous line), the term $\dfrac{\partial U}{\partial n}$ in (A.5) being approximated by the 2-D formula analog of (A.11) (resp., (A.13), (A.15)). As shown in Figure A.3, if $\dfrac{\partial U}{\partial n}$ is obtained from the Green's formula (A.15) the two curves are identical; this approximation leads to a better accuracy.

In Figure A.4, the exact RCS (dotted line) is compared with the RCS of the computed solution (continuous line).

A.3.2 3-D Numerical experiments

The same comparisons have been carried out in 3-D with a sphere as obstacle. The radius of the sphere is λ and the artificial boundary is located at a distance λ to ∂B. With the angles defined as in Figure 7.12, the incident wave is defined by $\varphi = 270°$.

The mesh consists of about 88,000 nodes and 500,000 tetrahedra.

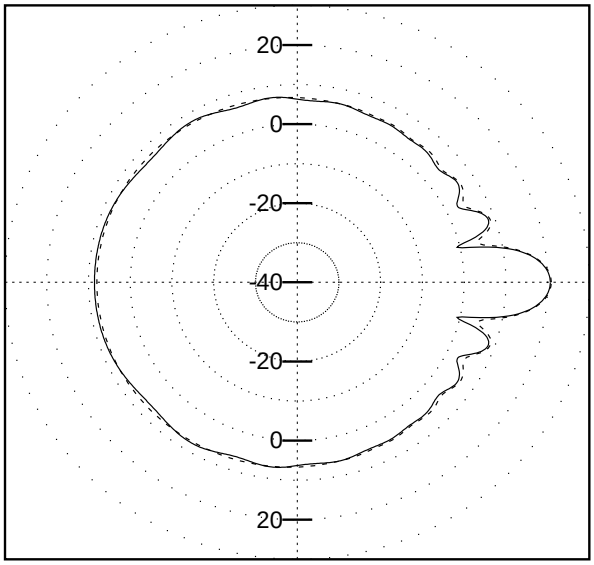

Figure A.1: Cylinder: comparaison of exact RCS and exact solution's computed one ($\frac{\partial U}{\partial n}$ constant on each edge).

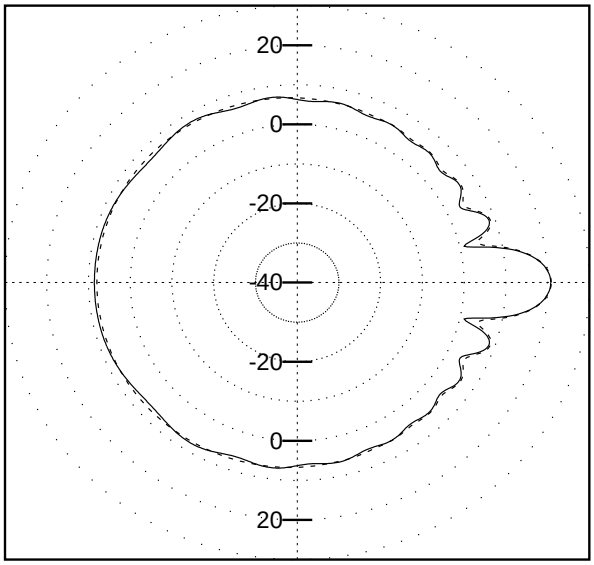

Figure A.2: Cylinder: comparaison of exact RCS and exact solution's computed one ($\frac{\partial U}{\partial n}$ defined by averaging at each node).

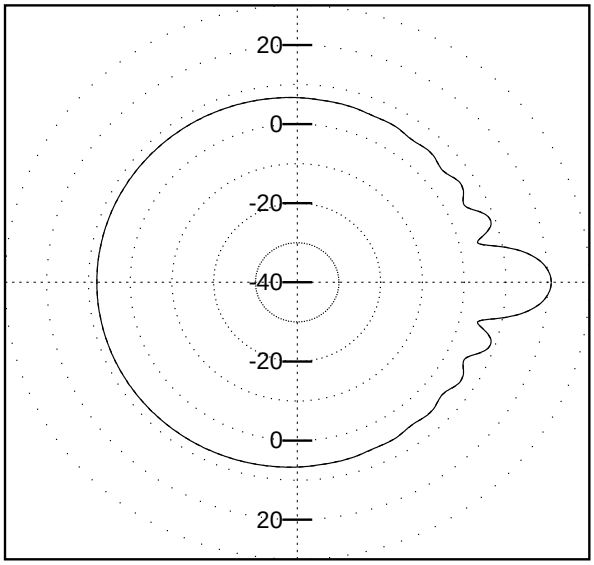

Figure A.3: Cylinder: comparaison of exact RCS and exact solution's computed one ($\frac{\partial U}{\partial n}$ obtained by Green's formula).

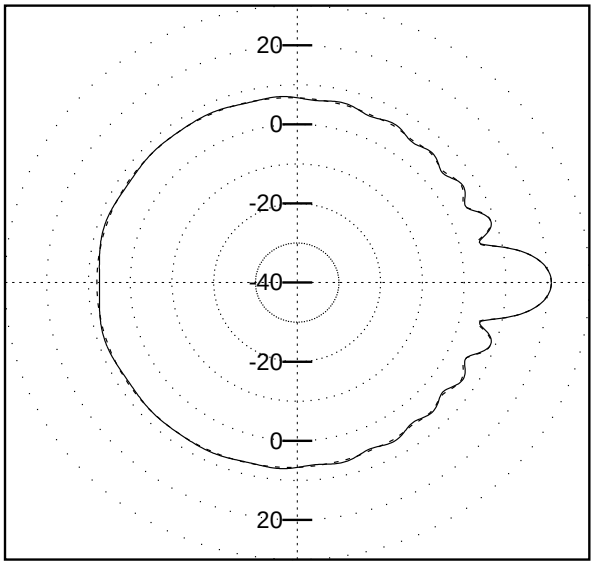

Figure A.4: Cylinder: comparaison of exact RCS and computed solution's one ($\frac{\partial U}{\partial n}$ obtained by Green's formula).

In Figure A.5 (resp., A.6, A.7), we compare, in the plane $(y = 0)$, the exact RCS (dotted line) with the exact solution's computed RCS (continuous line), the term $\frac{\partial U}{\partial n}$ in (A.8) being computed by (A.11) (resp., (A.13), (A.15)).

As in the 2-D case, we notice that the discretization of $\frac{\partial U}{\partial n}$ via a Green's formula leads to a good accuracy.

In Figure A.8, we compare also the exact RCS (dotted line) with the RCS of the computed solution (continuous line).

For the RCS computations presented in Section 7.6, we have used approximation (A. 15).

References

[1] I. Lasiecka, R. Triggiani, eds., *Control Problems for Systems described by Partial Differential Equations and Applications,* Lectures Notes in Control and Information, Vol. 97 (Springer, Berlin, 1987).

[2] G. Auchmuty, E.J. Dean, R. Glowinski and S.C. Zhang, Control Methods for the Numerical Computation of Periodic Solutions of Autonomous Differential Equations, in *Control Problems for Systems described by Partial Differential Equations and Applications*, I. Lasiecka, R. Triggiani eds, Lecture Notes in Control and Information, Vol. 97 (Springer, Berlin, 1987), pp. 64-89.

[3] M.O. Bristeau, R. Glowinski and J. Périaux, Scattering Waves using Exact Controllability Methods, *31st AIAA Aerospace Sciences Meeting, Reno, Nevada,* AIAA Paper 93-0460.

[4] M.O. Bristeau, R. Glowinski and J. Périaux, Using Exact Controllability to solve the Helmholtz Equation at High Wave Numbers, in *Mathematical and Numerical Aspects of Wave Propagation*, T. Kleinman, Th. Angell, D. Colton, F. Santosa and I. Stakgold eds (SIAM, Philadelphia, PA, 1993), pp. 113-127.

[5] R. Glowinski, J.L. Lions, Exact and Approximate Controllability for Distributed Parameter Systems, Part II *Acta Numerica*, 1996, pp. 159-333.

[6] M.O. Bristeau, E.J. Dean, R. Glowinski, V.K. Kwok, J. Périaux, Application of Exact Controllability to the Computation of Scattering Waves, in *Control Problems in Industry,* I. Lasiecka, B. Morton eds (Birkhauser,Boston, 1995), pp. 17-41.

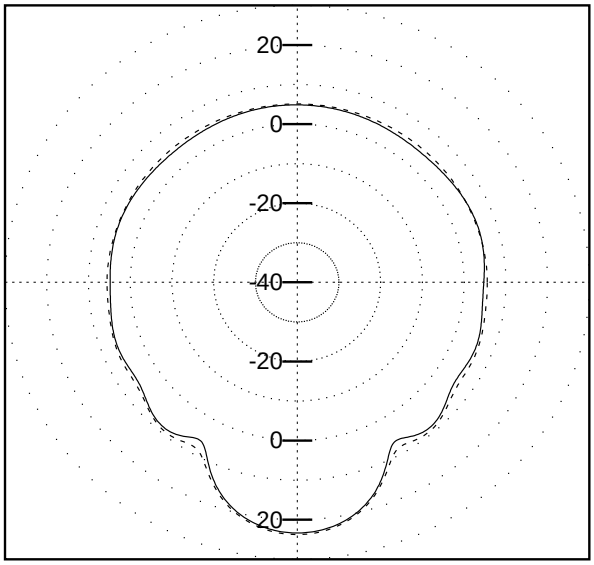

Figure A.5: Sphere: comparaison of exact RCS and exact solution's computed one ($\frac{\partial U}{\partial n}$ constant on each face).

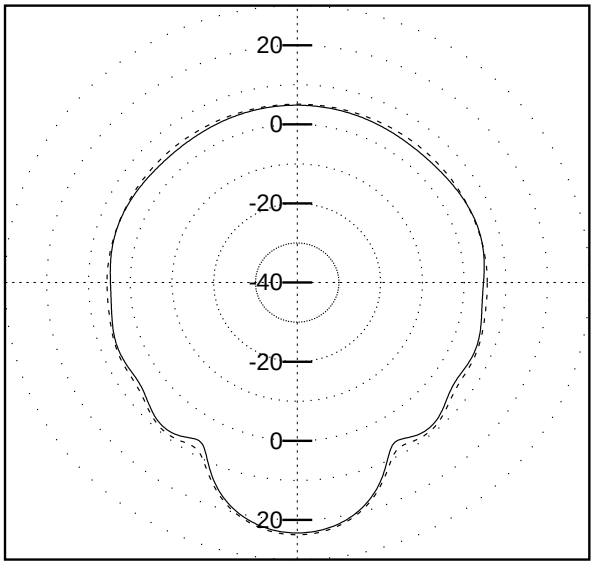

Figure A.6: Sphere: comparaison of exact RCS and exact solution's computed one ($\frac{\partial U}{\partial n}$ defined by averaging at each node).

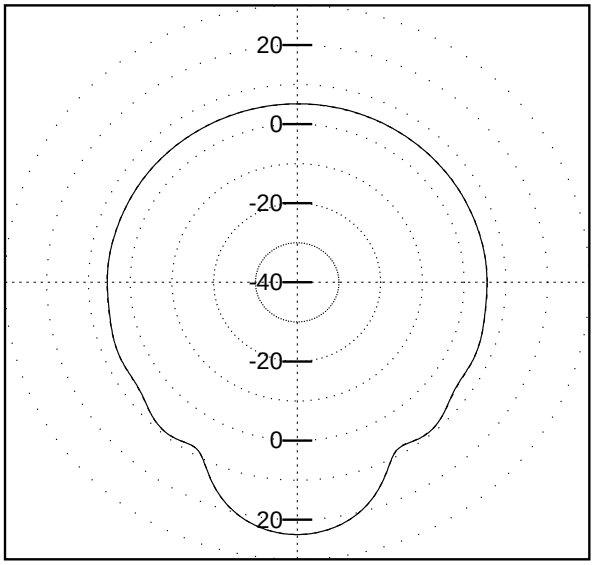

Figure A.7: Sphere: comparaison of exact RCS and exact solution's computed one ($\frac{\partial U}{\partial n}$ obtained by Green's formula).

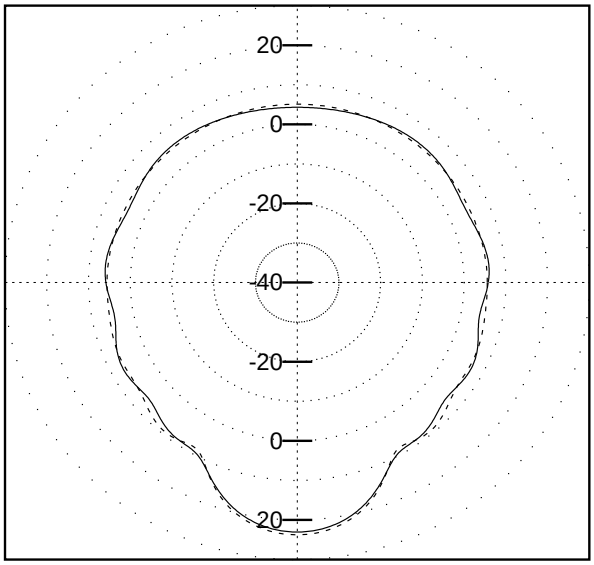

Figure A.8: Sphere: comparaison of exact RCS and computed solution's one ($\frac{\partial U}{\partial n}$ obtained by Green's formula).

[7] G. Auchmuty, Control theoretic methods for the computation of special solutions of differential equations, in *Computational Sciences for the 21 st Century*, M.O. Bristeau, G. Etgen, W. Fitzgibbon, J.L. Lions, J. Périaux, M.F. Wheeler eds. (Wiley, Chichester, 1997), pp. 655-659.

[8] C. Bardos, J. Rauch, Variational algorithms for the Helmholtz equation using time evolution and artificial boundaries. *Asymptotic Analysis, 9*, 1994, pp. 101-117.

[9] M.O. Bristeau, R. Glowinski, J. Périaux, Exact Controllability to solve the Helmholtz Equation with Absorbing Boundary Conditions,in *Finite Element Methods,* D. Krizek, P. Neittaanmaki, R. Stenberg eds (M. Dekker Inc., New-York, 1994), pp. 79-93.

[10] J.L. Lions, Exact Controllability, Stabilization and Perturbation for Distributed Systems, *SIAM Rev.*, 30, 1988, pp. 1-68.

[11] J.L. Lions, *Contrôlabilité Exacte, Perturbation et Stabilisation des Systèmes Distribués,* Vols 1 and 2, (Masson, Paris, 1988).

[12] J. Erhel, Sparse matrix multiplication on vector computers, *Int. J. of High Speed Computing*, Vol. 2, N° 2, 1990, pp. 101-116.

[13] P.L. George, E. Seveno, Génération de Maillages par une Méthode de Type Frontal, *INRIA Report N° 1725*, 1992.

[14] E. Seveno, Towards an adaptive advancing front method, *Proc. of 6th Int. Meshing Roundtable*, Park City, Utah, (1997).

[15] E. Seveno, Génération automatique de maillages tridimensionnels isotropes par une méthode frontale, Thèse Univ. P. & M. Curie, 1998.

[16] J. Erhel, F. Guyomarch, An augmented subspace conjugate gradient, *INRIA Research Report N° 3278*, 1997.

[17] M.O. Bristeau, J. Erhel, Augmented Conjugate Gradient. Application in an iterative process for the solution of scattering problems, to appear.

[18] G. Mur, The Finite Element Modeling of Three Dimensional Electromagnetic Fields using Edge and Nodal Elements, *IEEE Trans. in Antennas and Prop.,* Vol. 41, n° 7, 1993, pp. 948-953.

[19] *Proceedings of the 3rd Workshop on Approximations and Numerical Methods for the solution of Maxwell equations*, F. El Dabaghi, K. Parrott, H. Steve eds. (J. Wiley & Sons, Chichester), to appear.

[20] Y. Kuznetsov, K. Lipnikov, On the application of fictitious domain and domain decomposition methods for scattering problems on Cray Y-MP C98, *Tech. Report 9557, Department of Mathematics*, University of Nijmegen, Nijmegen, The Netherlands, December 1995.

[21] M.O. Bristeau, Exact Controllability methods for calculation of 3D time-periodic Maxwell solutions, in *Computational Science for the 21st Century*, M.O. Bristeau, G. Etgen, W. Fitzgibbon, J.L. Lions, J. Périaux and M.F. Wheeler eds. (Wiley, Chichester, 1997), pp. 492-503.

[22] M. Berggren, R. Glowinski, J.L. Lions, A computational approach to controllability issues for flow-related models (I) : Pointwise control of the viscous Burgers equation, *Int. J. Comput. Fluid Dynamics*, 7, 1996, pp. 237-252.

[23] J.J. Bowman, T.B.A. Senior, P.L.E. Uslenghi, *Electromagnetic and Acoustic Scattering by Simple Shapes*, Hemisphere Pub. Corp., 1987.

[24] C. Atamian, Résolution de problèmes de diffraction d'ondes acoustiques et électromagnétiques en régime fréquentiel par une méthode de domaines fictifs, Thèse Univ. P. & M. Curie, 1991.

Unit´e de recherche INRIA Lorraine, Technopôle de Nancy-Brabois, Campus scientifique,
615 rue du Jardin Botanique, BP 101, 54600 VILLERS LÈS NANCY
Unit´e de recherche INRIA Rennes, Irisa, Campus universitaire de Beaulieu, 35042 RENNES Cedex
Unit´e de recherche INRIA Rhône-Alpes, 655, avenue de l'Europe, 38330 MONTBONNOT ST MARTIN
Unit´e de recherche INRIA Rocquencourt, Domaine de Voluceau, Rocquencourt, BP 105, 78153 LE CHESNAY Cedex
Unit´e de recherche INRIA Sophia-Antipolis, 2004 route des Lucioles, BP 93, 06902 SOPHIA-ANTIPOLIS Cedex

Éditeur
INRIA, Domaine de Voluceau, Rocquencourt, BP 105, 78153 LE CHESNAY Cedex (France)
http://www.inria.fr
ISSN 0249-6399